DOI:
10.1016/j.jsv.2019.05.046

Document Version
Peer reviewed version

Adaptive fuzzy control of a magnetorheological elastomer vibration isolation system with time-varying sinusoidal excitations

Jie Fu[1], Junfeng Bai[1], Junjie Lai[1], Peidong Li[1], Miao Yu[1], Hak-Keung Lam[2]

1. Key Lab for Optoelectronic Technology and Systems, Ministry of Education, College of Optoelectronic Engineering, Chongqing University, Chongqing 400044, China
2. Department of Informatics, King's College London, Bush House, Strand campus, 30 Aldwych, London, WC2B 4BG, United Kingdom

Email: fujie@cqu.edu.cn

Abstract: This paper presents the design method of an adaptive fuzzy controller (AFC) for a magnetorheological elastomer (MRE) vibration isolation system with time-varying sinusoidal excitations. In the first place, Kelvin model of MRE isolator without application of driving current is obtained by acceleration sweep experiments on a shake table, which establishes a foundation for the design of adaptive law. Secondly, a semi-active AFC with factor adjustment mechanism is designed based on the transmissibility curves under zero magnetic application and semi-active fuzzy control theory, which is independent of the isolation system model and adaptive to time-varying excitations in amplitudes and frequencies without adopting complicated fast Fourier transformation (FFT) analyzer. Finally, acceleration responses of the system with AFC to time-varying sinusoidal excitations are evaluated by numerical simulation and physical experiments, which indicate that the AFC could maintain satisfying control effect in the presence of time-varying sinusoidal excitations in amplitudes and frequencies, and is also more optimal than conventional fuzzy controller (FC).

Keywords: magnetorheological elastomer (MRE), transmissibility curve, adaptive fuzzy controller (AFC), time-varying excitations, vibration isolation

1. Introduction

To guarantee the machining accuracy and measuring sensitivity, high-tech manufacturing facilities and instruments require a normal working environment with ultra-low vibrations [1-3]. The allowable maximum vibration velocity of a grating-ruling engine, the grating constant of which is 1/6000 mm, is 5 μm/s. And the scanning speed of a scanning electron microscopy, the magnification of which is 140

thousand, is 30 μm/s. Generally, the vibration in the precision platform with grating-ruling engine is produced by earth's rotation, change of earth's crust, building swinging, transformer and motor operating, and occupant movement, and so on, and the corresponding frequency range is about 0-100Hz. To isolate the above sensitive equipment from multiple vibration sources in the working environment, passive mounts such as air/pneumatic springs and rubber isolators are widely installed. However, the passive ones would amplify low-frequency vibrations and have a poor environmental adaptability [4].

As a branch of MR materials, MRE is composed of polymer and ferromagnetic particles, the mechanical features of which including storage modulus and loss modulus could be adjusted by the external magnetic field [5-8]. Through controlling the target structure's stiffness and damping in real-time, the MRE based semi-active isolator could suppress the load's vibration, which is transmitted from the base, and thus has attracted a great deal of exploration on its potential applications on vehicle suspension [9-12], sensitive equipment [13-17], civil structure [18-23] and flexible structure [24, 25]. Moreover, there are experiments showing that the MRE with small strain can obtain a more obvious MR effect and better controllability than the one with greater strain [26]. Therefore, the MRE is more suitable for the inhibition of micro-amplitude vibrations.

The vibration isolation performance only depends on the control strategy for the isolation system with fixed isolator structure in practical application. Based on the relationship of control strategy and system model, there are two kinds of methods namely model-dependent and model-free on MRE isolation control system. The former includes H_∞ control [9], Lyapunov-based control [20], clipped-optimal control [27], LQR [23]. However, the accurate inverse isolator model is always required. Actually, it is a challenge to obtain an accurate inverse mode with nonlinear hysteretic behavior. Mode-free method such as ON-OFF control [11, 21, 28] and fuzzy control [16, 22], provides the solution for the problem. The ON-OFF control has the advantage of simple structure and easy implementation for real-time control applications. However, it makes the response of the system more oscillatory [16], which leads to unsatisfied results of vibration isolation. As a nonlinear controller, the model-free fuzzy control is independent of the isolator's complicated inverse model, and has also demonstrated strong robustness [29-31]. Fu *et al* [16] solved the problem of micro-vibration control of a quarter precision platform with an MRE isolator and

FC, and the acceleration transmissibility was reduced by 54.04% at most in experimental implement. Li *et al* [22] adopted an FC to compute the MRE isolators' driving currents to isolate the building model from the motion induced by a scaled EI Centro earthquake. However, when the sinusoidal excitations vary in amplitude and frequency, the FCs above with fixed quantification factors, scaling factors, rules and membership functions, which are not of adaptive ability, cannot guarantee stability and satisfactory control specifications. Thus the AFC is required to deal with the problem [32-34]. It is easier to tune the gains of quantification and scaling factors, and it also affects the system performance greatly than the rule base and membership functions [35], so gain-tuning rather than rule-tuning and membership-function-tuning is chosen in this work to construct an AFC. It is worth mentioning that MRE isolator is a variable stiffness device, the controlled output force generated by the isolator is not only dependent on excitation amplitude, but also sensible for varying excitation frequency [36], so the control law is required to be adaptive for both time-varying amplitude and frequency. However, the adaptive methods in published papers are not relevant to the MRE isolation system with time-varying excitation. It is still a task to design the adaptive law for MRE isolation system with time-varying amplitude and frequency excitation.

Consequently, the main contribution of this work is to propose a semi-active AFC for time-varying excitation in amplitude and frequency and verify excellent vibration control performance of the proposed controller by experiments. The control force associated with the AFC is generated by adopting the MRE isolator and quarter precision platform system subjected to time-varying sinusoidal vibrations. The Kelvin model of MRE isolator without application current is identified in Section 2. In section 3, an AFC is designed, and the adaptive law (factor adjustment mechanism) is constructed, which make the factors adaptive to excitation frequency and amplitude through adopting the passive Kelvin model and simple peak observer rather than the complicated FFT analyzer. And numerical simulations and experimental verification are conducted in Section 4 and Section 5 to explore the performance of the proposed AFC, respectively. Finally, the conclusions are summarized in Section 6.

2. Kelvin model of MRE isolator

The shear-compression mixed mode MRE isolator employed in this paper is shown in Fig. 1. Detailed parameters and structure of the isolator can be found in [16].

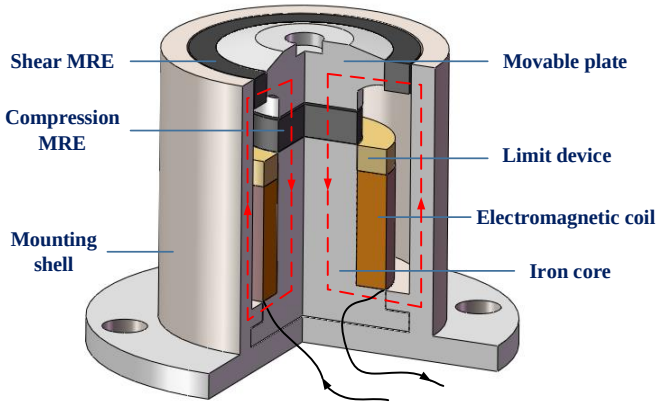

Fig. 1. Structure of the mixed mode MRE isolator

Kelvin model (passive model) of MRE isolation system with zero magnetic fields is shown in Fig.2 and the corresponding dynamic equation can be described as

$$m\ddot{x}_2(t) = k_0(x_1(t) - x_2(t)) + c_0(\dot{x}_1(t) - \dot{x}_2(t)) \tag{1}$$

where m represents the mass of the isolation structure. k_0 and c_0 are the isolator stiffness and damping coefficient without magnetic field application, respectively. $x_1(t)$ and $x_2(t)$ are the displacement of the base and isolation structure, respectively.

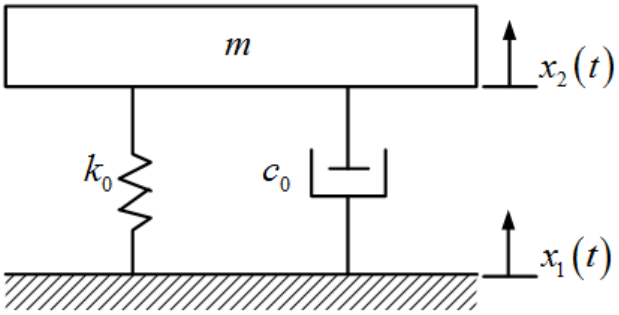

Fig. 2. Kelvin model of MRE isolation system

In order to identify the stiffness and damping coefficient and obtain the Kelvin mode of MRE isolator, the acceleration sweep frequency experimental system for the MRE isolator is set up in Fig. 3, where $m = 1.2\text{kg}$. The experimental result is shown in blue line in Fig. 4.

According to Fig. 4 and the identified method of Kelvin model [37], the parameters, such as stiffness and damping coefficient of MRE isolation system are shown in Table 1, and identified model when the driving current is 0 A, follows

$$T_{\text{passive}}(\text{s}) = \frac{702.4s + 678336}{1.2s^2 + 702.4s + 678336} \tag{2}$$

where $T_{\text{passive}}(s)$ is the system transfer function of the response acceleration (the acceleration of the isolation structure) and the excitation acceleration.

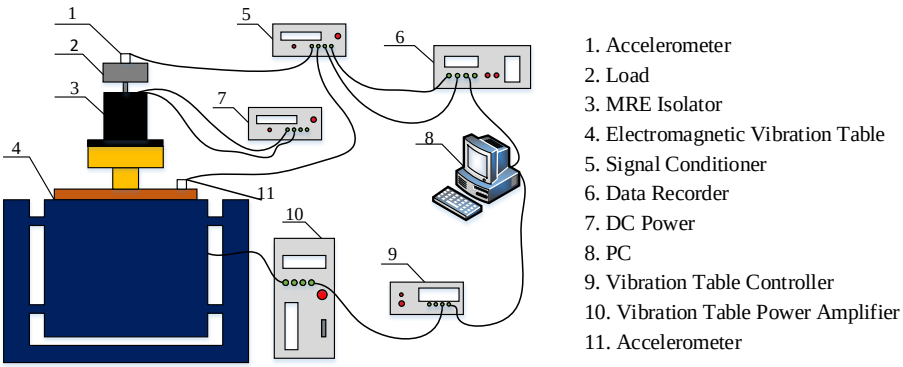

(a)

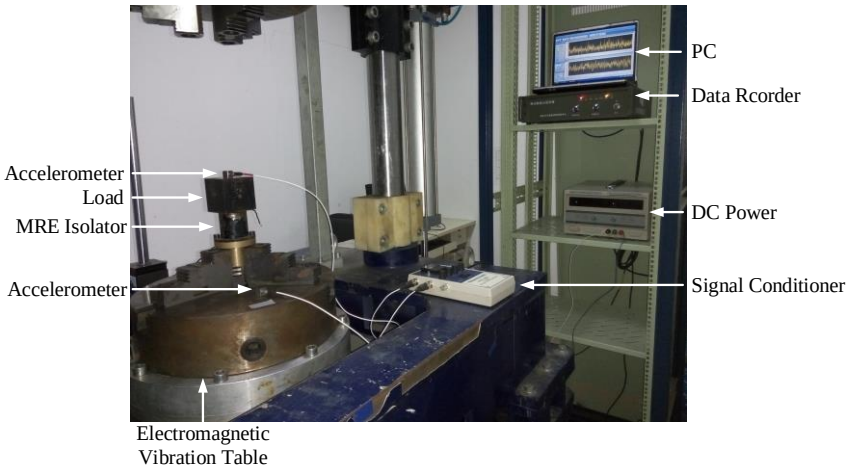

(b)

Fig. 3. Acceleration Sweep frequency experimental system: (a) sketch; (b) picture

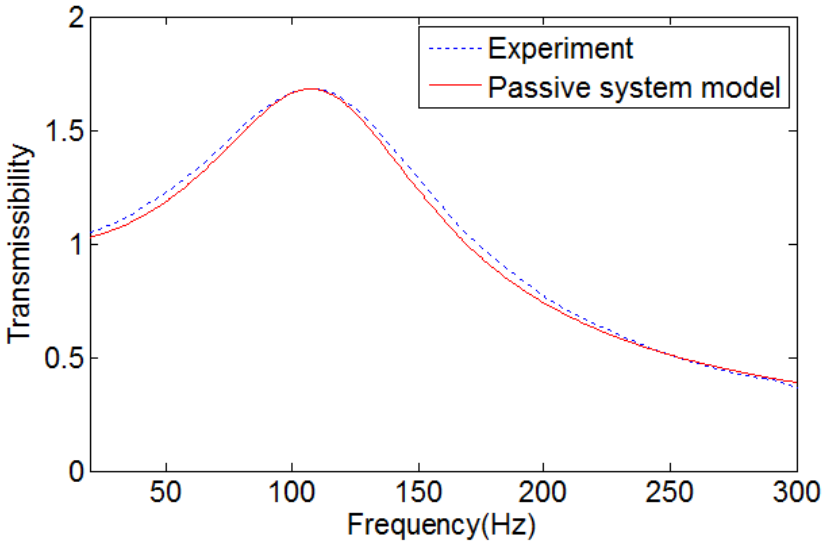

Fig. 4. Magnitude-frequency curves obtained from experiment and passive system model

Table 1 Parameters of MRE isolator under 0A

Resonance frequency(Hz)	Transmissibility peak value	Damping ratio	Natural frequency	Equivalent stiffness(kN/m)	Equivalent damping(N·s/m)
107.3	1.7	0.4	119.7	678.3	702.4

Fig. 4 compares the magnitude-frequency curves obtained from experiment and Equation (2), which indicates that the Kelvin model could describe the passive system's transmissibility characteristic closely and is suitable for forwarding modeling of the passive system with zero magnetic field.

The test results also provide the identified parameter values and controllable frequency range of the MRE isolation system for controller design (adaptive law design) which are described in the following section.

3. Semi-active adaptive fuzzy controller (AFC) design

In this section, based on the vibration isolation principle of the MRE isolator and fuzzy control theory, a semi-active AFC is designed for MRE isolation system with time-varying sinusoidal excitations in amplitudes and frequencies.

3.1 Semi-active control law

The MRE vibration isolation system with the application of variable magnetic fields is shown in Fig. 5.

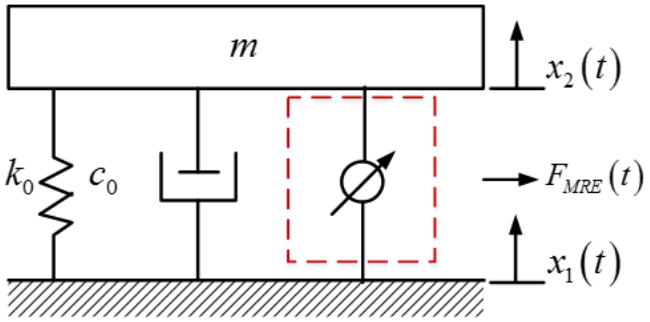

Fig. 5. Dynamic model of the MRE isolation system

Base on the Newton's motion law, the dynamic equation of the isolation system is derived as

$$m\ddot{x}_2(t) = k_0(x_1(t) - x_2(t)) + c_0(\dot{x}_1(t) - \dot{x}_2(t)) + F_{\mathrm{MRE}}(t). \tag{3}$$

The output force generated by MRE isolator $F_{\mathrm{MRE}}(t)$ is described by

$$F_{\mathrm{MRE}}(t) = \Delta k(x_1(t) - x_2(t)) + \Delta c(\dot{x}_1(t) - \dot{x}_2(t)). \tag{4}$$

where Δk is the increment stiffness under the electromagnetic field. Δc is the

increased damping coefficient under the electromagnetic field.

The semi-active control law is described as

$$F_{\mathrm{MRE}}(t)=\begin{cases}F_{\max} & x_2(t)x_r(t)\geq 0,\ F_c(t)\geq F_{\max}\\ F_c(t) & x_2(t)x_r(t)\geq 0,\ F_c(t)<F_{\max}\\ 0 & x_2(t)x_r(t)<0\end{cases} \tag{5}$$

where $F_{\max}$ is the maximum output force of the MRE isolator, $F_c(t)$ is the desired force computed by the designed AFC in the following section, and $x_r(t)=x_2(t)-x_1(t)$ is the relative displacement between the isolation structure and base. It can be also expressed by Fig. 6. When the product of the relative displacement $x_r(t)$ and isolation structure displacement $x_2(t)$ are positive (or when the movement of the two displacement is in the same direction), there has controlled force output (current application), otherwise, no output of controlled force (applied current). The detail derivation can be found in Ref. [16].

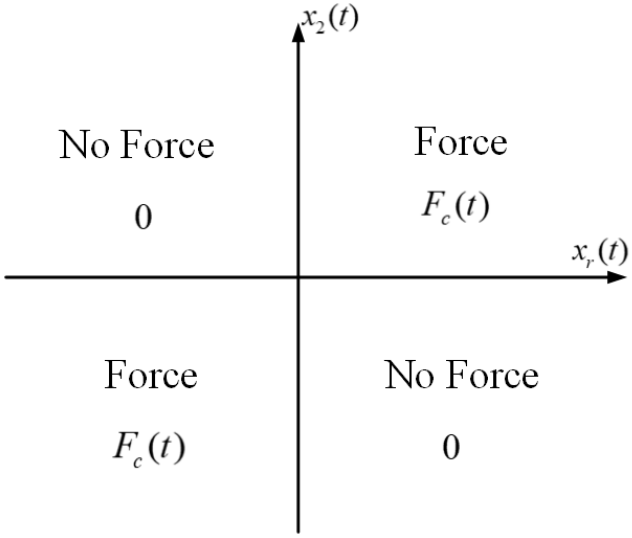

Fig. 6. Semi-active control law of MRE isolation system

3.2 Semi-active adaptive fuzzy controller (AFC)

For both the frequency and amplitude of the excitation signal are fixed, the conventional FC can deal with that well in [16]. However, as there are time-varying excitations in amplitudes and frequencies occurring in many practical applications, the conventional FC with constant factors may not be able to achieve satisfactory control effect. To improve the performance of the controlled system, the AFC with

factors on-line adaptive mechanism is designed. The structure of AFC vibration isolation system is shown in Fig. 7 where the AFC is enclosed by the dashed rectangle. Except for the conventional FC elements, the adaptive capability allows that the qualification and scaling factors can be regulated in real-time for time-varying excitations in amplitudes and frequencies, in which the passive system model follows Eq. (2) and the peak observer and adjustment mechanism are to be designed in the following section. So it will have more effective suppression ability for time-varying vibration.

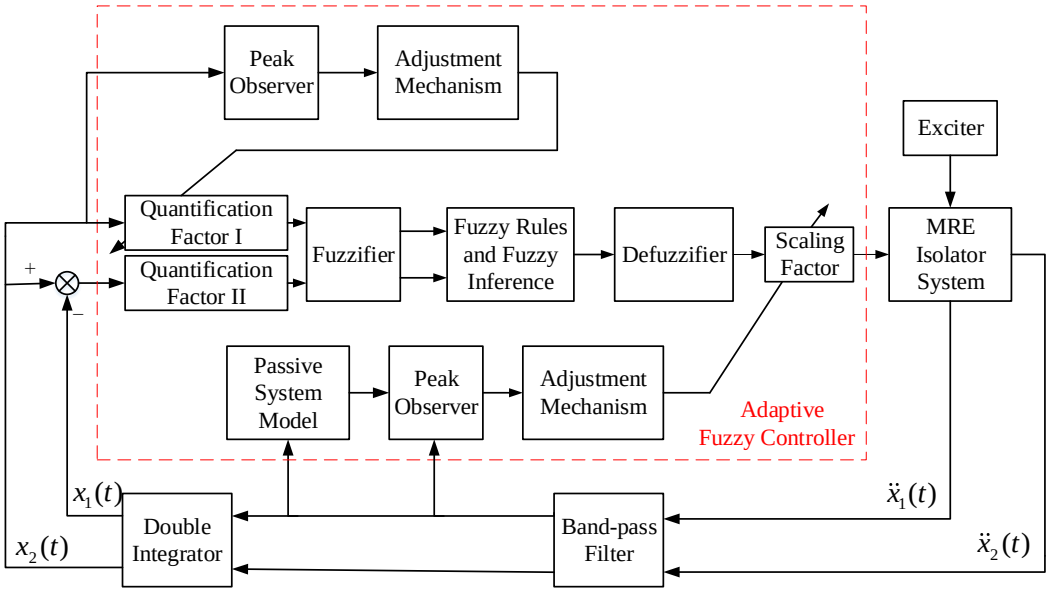

Fig. 7. Schematic diagram of AFC for MRE isolation system

3.2.1 Main structure of AFC

The AFC consists of conventional FC (fuzzifier, fuzzy rules and fuzzy inference and defuzzifier) and adaptive regulating mechanism, where the conventional FC parts are completely the same as that in [16]. A brief description of the input and output linguistic variables, fuzzy rules and membership function is given below. Readers are referred to [16] and references therein for details.

The input variables of the developed AFC are selected as relative displacement $x_r(t)$ between the isolation structure and base, and the isolation structure displacement $x_2(t)$, while the output is chosen as the force $F_{\mathrm{MRE}}(t)$ generated by MRE isolator. There are seven input and output linguistic variables, which are negative big (NB), negative medium (NM), negative small (NS), zero (ZO), positive small (PS), positive medium (PM), and positive big (PB). The discourse domain of the variables is [-7, 7].

D, RD and U are the isolation structure's displacement, the relative displacement and the output force in the fuzzy set, respectively.

Though it can be seen from Eq. (5), the semi-active control law (with or without output force of MRE isolator) depends on the product of the relative displacement and isolation structure's displacement. In fact, output force value mainly depends on the isolation structure's displacement, and the relative displacement is only used for checking whether or not the semi-active control law holds. Based on the above principle, the complete rule base is listed in Table 2. Taking an example that RD is NB, when D is NB, U has to be PB to suppress the change of D. And if D is positive, U must be zero to achieve the most optimal control effect for the isolation system.

Table 2. Fuzzy rules of the semi-active AFC.

U	RD						
	PB	PM	PS	ZO	NS	NM	NB
PB	NB	NB	NB	NB	ZO	ZO	ZO
PM	NM	NM	NM	NM	ZO	ZO	ZO
PS	NS	NS	NS	NS	ZO	ZO	ZO
D ZO	ZO	ZO	ZO	ZO	ZO	ZO	ZO
NS	ZO	ZO	ZO	PS	PS	PS	PS
NM	ZO	ZO	ZO	PM	PM	PM	PM
NB	ZO	ZO	ZO	PB	PB	PB	PB

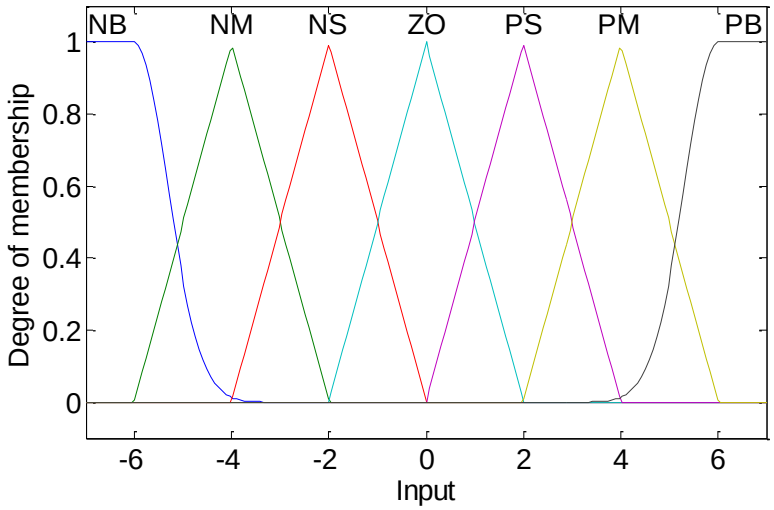

Fig. 8. The membership functions of input or output.

The membership functions of the inputs and output are same one, which are illustrated in Figures 8. The Gauss2mf-shaped membership function is employed for

NB and PB to enhance the smoothness of the MRE vibration control process and guarantee the system's stability, and the triangle-shaped membership function is selected for the rest of the linguistic variables to improve the sensitivity of the MRE vibration control system.

The fuzzy inference of the AFC is determined as Mamdani's method with the max-min composition. The membership functions of the inputs and output are same as that in [16].

3.2.2 Adaptive law

Different from the constant quantification factors set on specific signals in [16], the designed factors in this work are required to be adaptive for time-varying excitation. So the quantification factors' adaptation law follows

$$\begin{cases} k_1(t) = \dfrac{D_{\max}}{A_{x_2(t)}} \\ k_2(t) = \dfrac{RD_{\max}}{A_{x_r(t)}} = 2.8\times10^6 \end{cases} \tag{6}$$

where $D_{\max}$ and $RD_{\max}$ the maxima of the input discourse domain, which are 7 in this work, $A_{x_2(t)}$ and $A_{x_r(t)}$ the peak values of the isolation structure displacement and relative displacement (input variables), respectively. $k_1(t)$ represents the quantification factor of the isolation structure displacement, which is regulated in real time to ensure that the minimum and maximum of the scaled isolation structure displacement are -7 and 7, all the time. $k_2(t)$ is the quantification factor of the relative displacement of the isolation structure, as mentioned in the above section the relative displacement with little effect on the controlled output force value is only used for checking whether or not the semi-active control law holds, $k_2(t) = 2.8\times10^6$ keeps constant, which is obtained from numerical simulation.

When the quantification factors follow Eq. (6) and the excitation frequency is set, the scaling factor $k_3(t)$ shown below is homogeneous

$$k_3(t)\Big|_{\left(A_{x_1(t)}=n\cdot A_0\right)} = n\cdot k_3(t)\Big|_{\left(A_{x_1(t)}=A_0\right)} \tag{7}$$

where $A_{a_1(t)}$ is the peak value of the excitation acceleration $a_1(t)$, n is positive real number, A_0 is the peak value of unit excitation acceleration." in red color in revision version.

When the quantification factors follow Eq. (7) and the excitation amplitude is set as 1.0 m/s^2 ($A_0=1$), the optimal values of the scaling factor under different excitation frequencies are summarized in Table 3 which are achieved empirically through numerical simulation. Table 3 also lists the acceleration transmissibility $T_{\text{passive}}(s)$ of the passive MRE isolation system under different frequencies.

Table 3. The relationship among the excitation frequency, acceleration transmissibility and scaling factor

Excitation frequency (Hz)	Acceleration Transmissibility	Optimal Value of the scaling factor
80	1.51	0.20
90	1.62	0.21
100	1.70	0.24
110	1.72	0.28

The function of scaling factor and acceleration transmissibility is obtained by performing linear fitting on data from Table 3, which is shown in Fig. 9. It can be seen from figure that the scaling factor $k_3(t)$ and acceleration transmissibility T follows

$$k_3(t)\left|\left(A_{a_1(t)}=1.0\text{m/s}^2\right)=0.33T_{\text{passive}}(s)-0.30.\right. \tag{8}$$

The scaling factor's adaptation law for arbitrarily excitation acceleration can be obtained by combing Eqs. (7) and (8) together:

$$k_3(t)=0.33T_{\text{passive}}(s)\cdot A_{a_1(t)}-0.30A_{a_1(t)}. \tag{9}$$

For $A_{a_p}=T_{\text{passive}}(s)\cdot A_{a_1(t)}$, Eq. (9) can be written as

$$k_3(t)=0.33A_{a_p(t)}-0.30A_{a_1(t)} \tag{10}$$

where $A_{a_p(t)}$ is the peak value of the passive MRE system's response to the excitation acceleration.

To sum up, the adjustment mechanism of quantification factors and scaling factor or the adaptation law follows

$$\begin{cases} k_1(t) = \dfrac{7}{A_{x_2(t)}} \\ k_2(t) = 2.8\times 10^6 \\ k_3(t) = 0.33A_{a_p(t)} - 0.30A_{a_1(t)} \end{cases} \tag{11}$$

where $A_{x_2(t)}$, $A_{a_1(t)}$ and $A_{a_p(t)}$ are all obtained by the peak observer.

Therefore, the controlled output force of AFC follows

$$F_{\mathrm{MRE}}(t) = k_3(t)U \tag{12}$$

It is very difficult to find the scaling factor adaptive law dependent on both excitation amplitude and frequency. For the each optimal value of the scaling factor and acceleration transmissibility of the passive MRE isolation system are all relevant to different excitation frequency in Table 3, by linear fitting of the acceleration transmissibility and scaling factor, the scaling factor adaptive law with implicit frequency is obtained. The advantage of the designed adaptation law with amplitude and frequency adaptivity is that there is no need identifying the excitation frequency in real time control, which is a trouble thing. So the problem of time-varying frequency adaptation can be solved without complicated FFT analyzer.

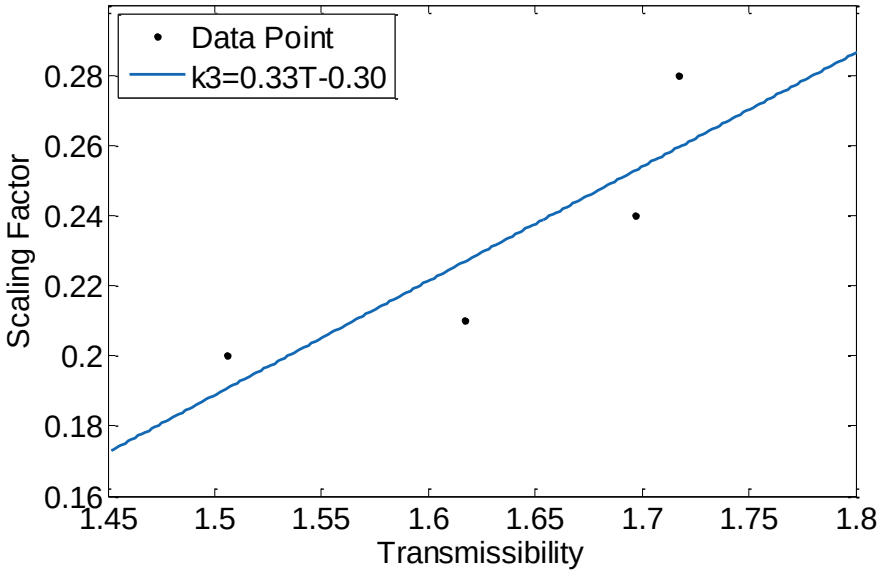

Fig. 9. Linear fitting of the acceleration transmissibility and scaling factor

3.2.3 Peak observer

The peak observer in Fig. 7 computes the peak value $A_{x(t)}$ of the time-varying input

signal $x(t)$ (displacement or acceleration) in real time by

$$A_{x(kT)}=\begin{cases}|x(kT-T)| & [x(kT)-x(kT-T)][x(kT-T)-x(kT-2T)]\le 0,|x(kT-T)|\neq 0\\ |x(kT)| & [x(kT)-x(kT-T)][x(kT-T)-x(kT-2T)]>0,|x(kT)|>A_{x(kT-T)}\\ A_{x(kT-T)} & \text{Other}\end{cases} \quad (13)$$

where $A_{x(kT)}$ is the peak value at sampling time kT, T is the sampling period of the control system, $k\in N$. Fig. 10 illustrates how to obtain the peak value of input signal by peak observer. It can been seen that in the case with the negative product of $x(kT)-x(kT-T)$ and $x(kT-T)-x(kT-2T)$, there follows that $[x(kT)-x(kT-T)][x(kT-T)-x(kT-2T)]\le 0$ and the peak value of input signal is $|x(kT-T)|$. In the case with $[x(kT)-x(kT-T)][x(kT-T)-x(kT-2T)]>0$ and $|x(kT)|>A_{x(kT-T)}$, the peak value is $|x(kT)|$, otherwise, the peak value is kept as $A_{x(kT-T)}$.

The effectiveness of the above AFC will be verified in the following section.

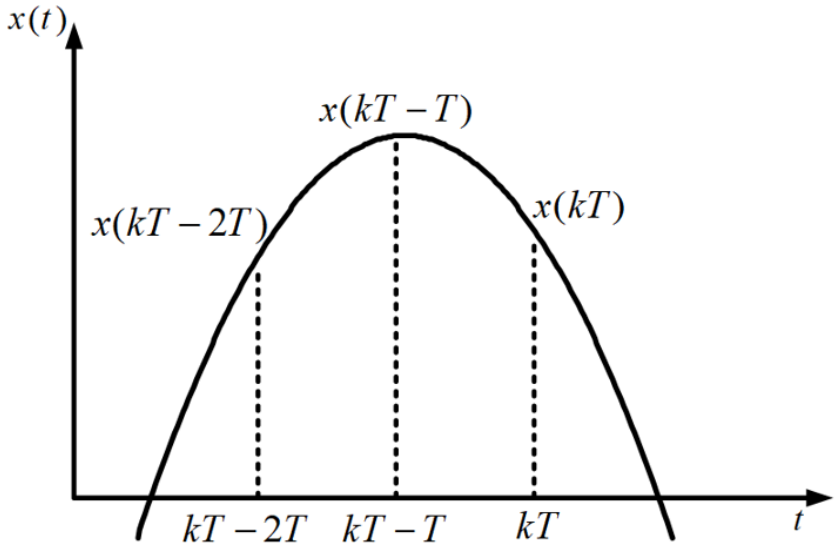

Fig. 10. Principle of peak observer

4. Numerical simulation and discussion

Considering the time-varying excitation in amplitudes and frequencies, numerical simulations are conducted in MATLAB software to explore the performance of the designed AFC under sinusoidal excitations with variable amplitudes and frequencies. Meanwhile, the control effectiveness comparison with conventional FC is carried out,

where the conventional FC's quantification and scaling factors are regulated according to the 80 Hz excitation with the amplitude 1.0 m/s^2 and kept constant. In addition, acceleration decrease is defined in this paper to quantify the vibration attenuation effect as follows:

$$\Delta a = \frac{a_{RMS(Semi-active)} - a_{RMS(passive)}}{a_{RMS(passive)}} \tag{14}$$

where $a_{RMS(Semi-active)}$ and $a_{RMS(passive)}$ are the acceleration Root Means Square (RMS) of the isolation structure with semi-active control and passive control, respectively.

4.1 Amplitude-varying excitation

The amplitude of the 80 Hz excitation increases from 1.0 m/s^2 to 4.0 m/s^2 in 10 seconds linearly, and the regulation processes of the AFC's quantification factor I, scaling factor and control force are shown in Fig. 11. Fig. 12 compares the responses and percentage decreases of the isolation structure's acceleration under the AFC and conventional one.

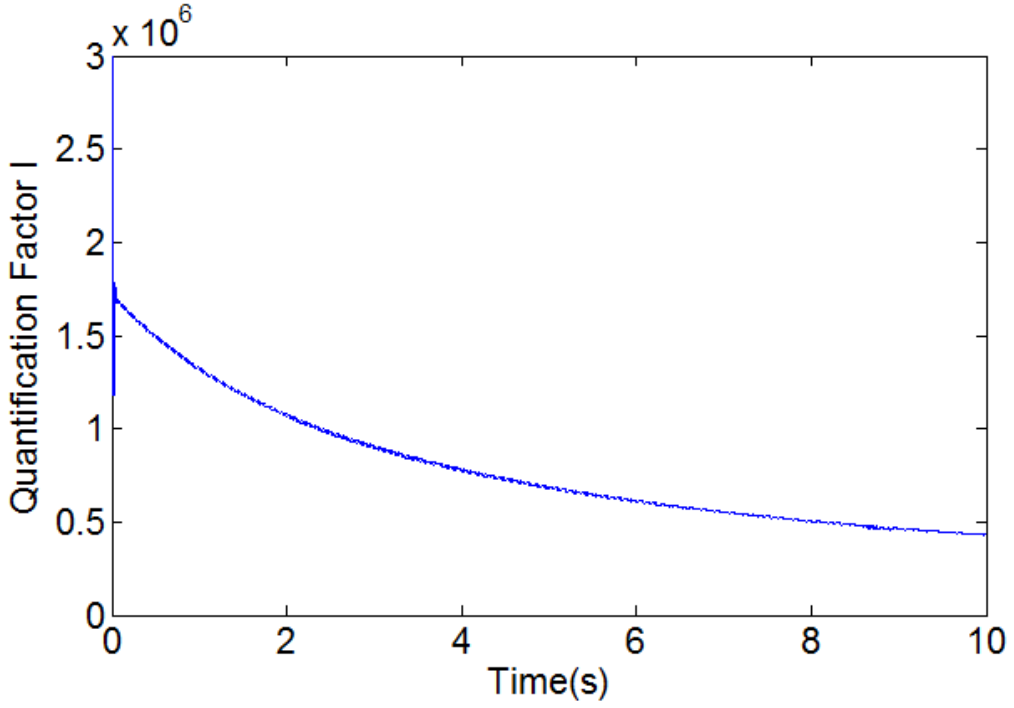

(a)

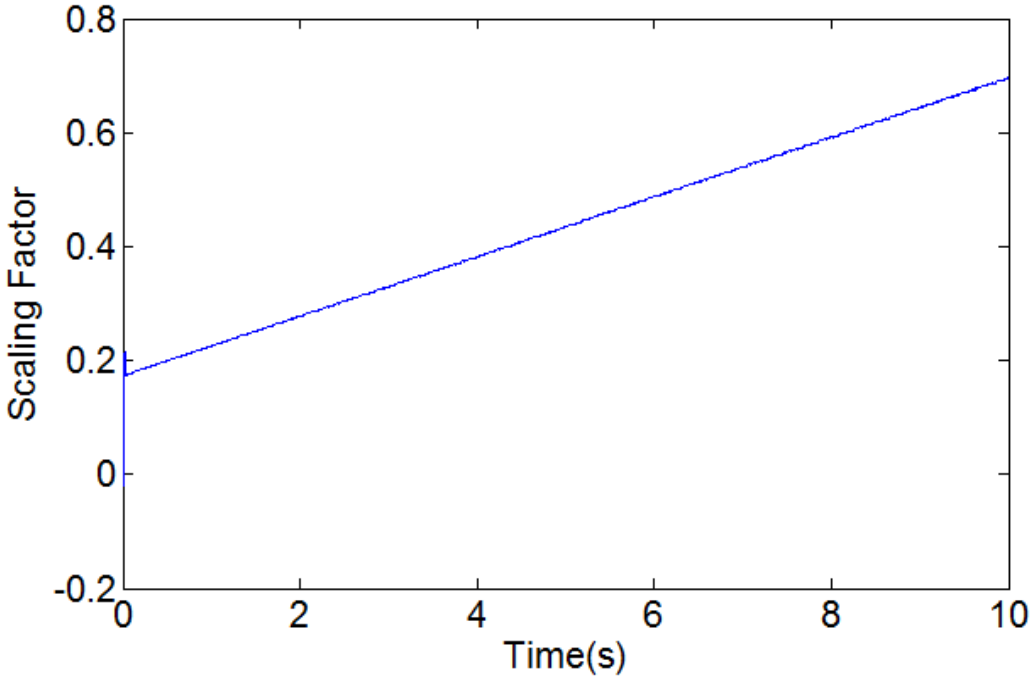

(b)

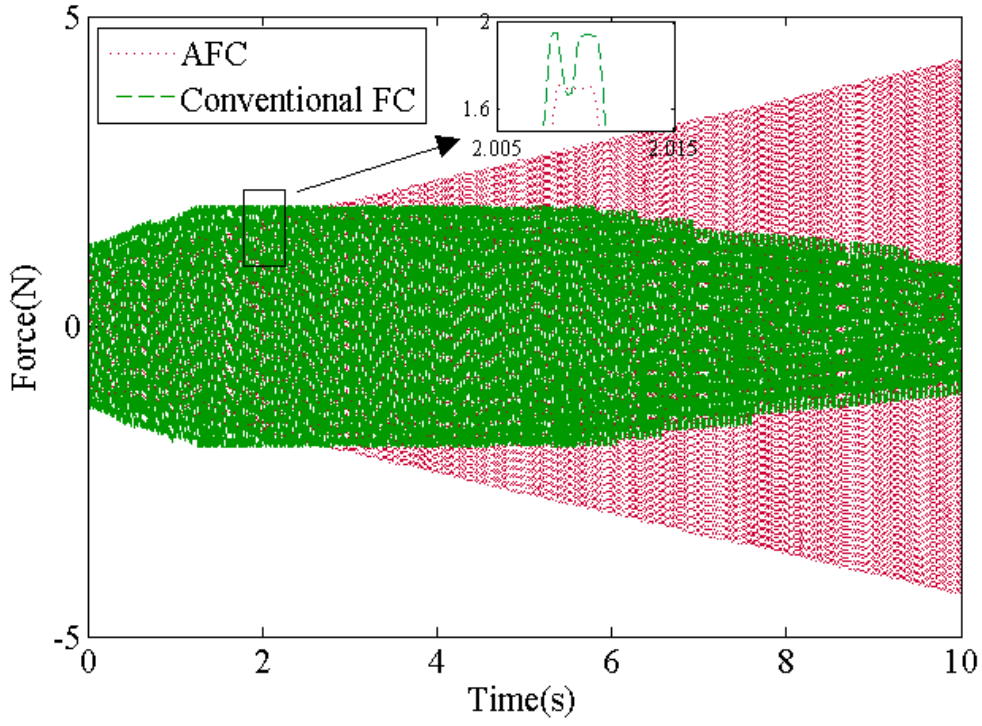

(c)

Fig. 11. Regulation processes of the AFC's factors under amplitude-varying excitation: (a) quantification factor I, (b) scaling factor, and (c) output force of controller

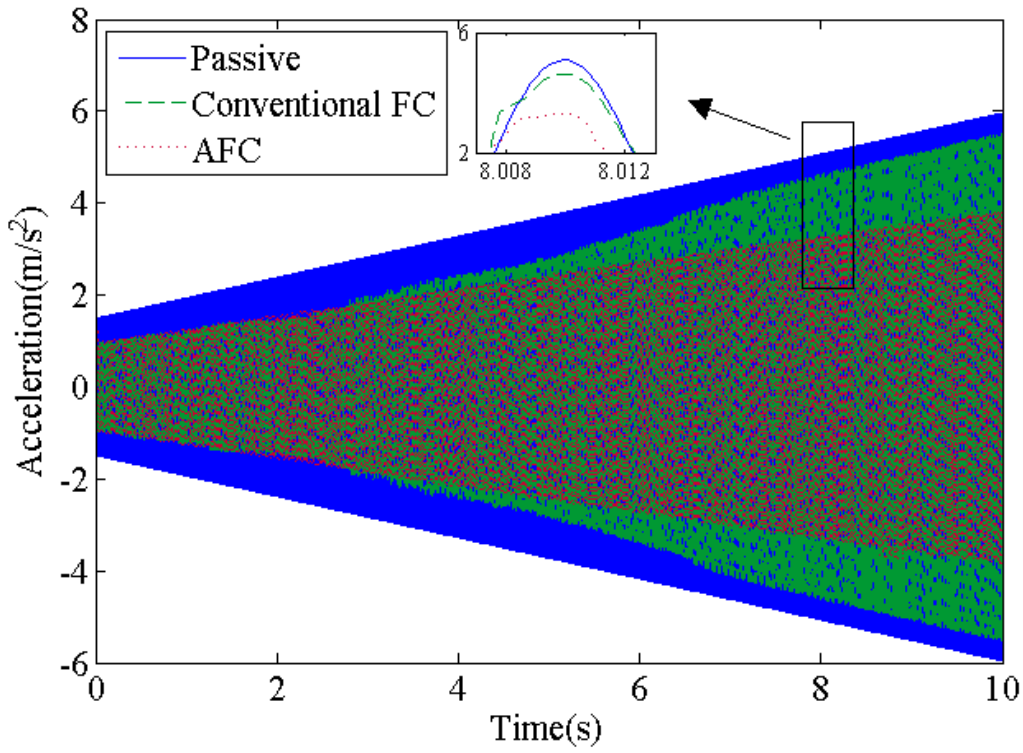

(a)

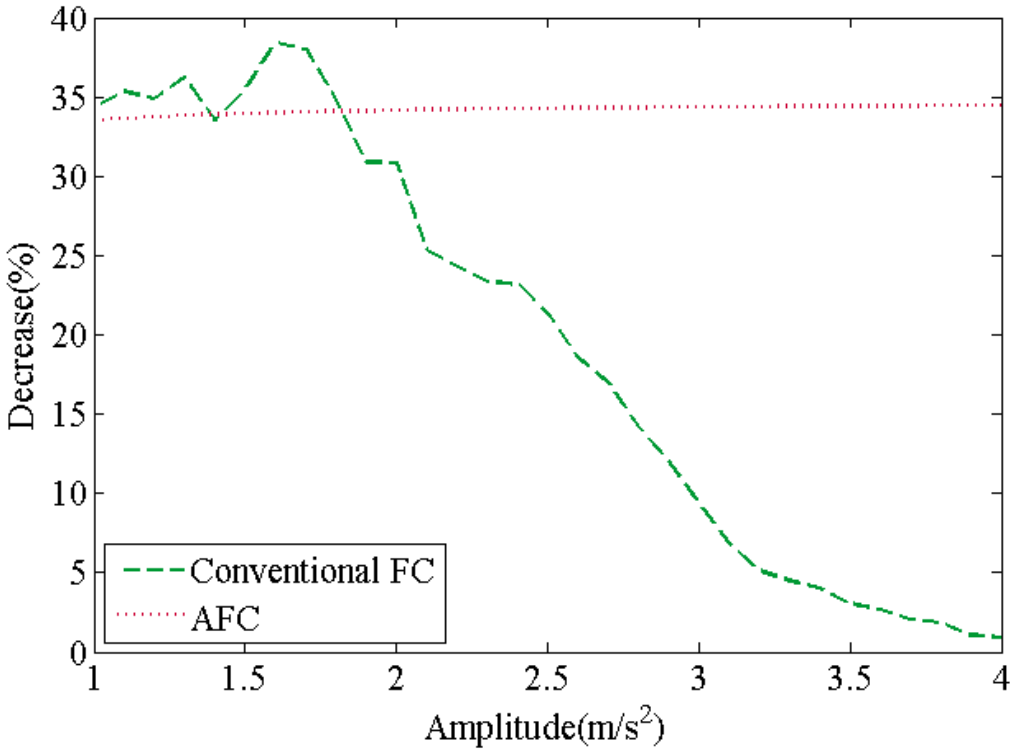

(b)

Fig. 12. The isolation structure's acceleration under different controllers and amplitude-varying excitation: (a) responses in time domain, and (b) percentage decreases

It can be seen from Figs 11 and 12 that the conventional FC with constant factors

could only achieve the satisfactory control effect when the excitation signal is with no change or a small variation (1-2 m/s^2). However, when the excitation amplitude is increasing, the vibration suppress with conventional FC is decreasing sharply. For instance, when the acceleration amplitude increases to 4.0 m/s^2, the percentage decrease is just 0.93%. And the one of the AFC remains around 34%. The reason is that adjustment mechanism proposed in Eq. (11) in this work makes the output of the AFC be adaptive with the changeable amplitude and fixed frequency.

4.2 Frequency-varying excitation

The frequency of the 1.0 m/s^2 excitation increases from 80 to 110 Hz in 10 seconds linearly, and the regulation processes of the AFC's quantification factor I, scaling factor and control force are shown in Fig. 13. And Fig. 14 compares the responses and percentage decreases of the isolation structure's acceleration under different controllers. It can be seen from Fig. 14 that the AFC could effectively attenuate the vibrations of the isolation structure in both resonant and non-resonant frequencies due to the adaptive law application with implicit frequency, which also verifies that frequency has effect on the vibration suppression and should be considered in controller design, and is more optimal than the conventional FC.

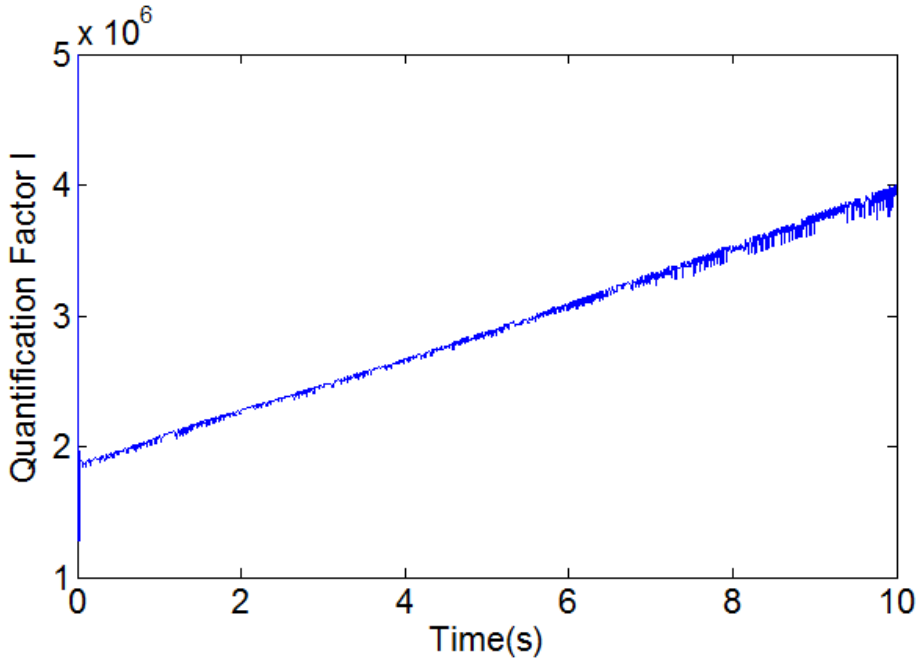

(a)

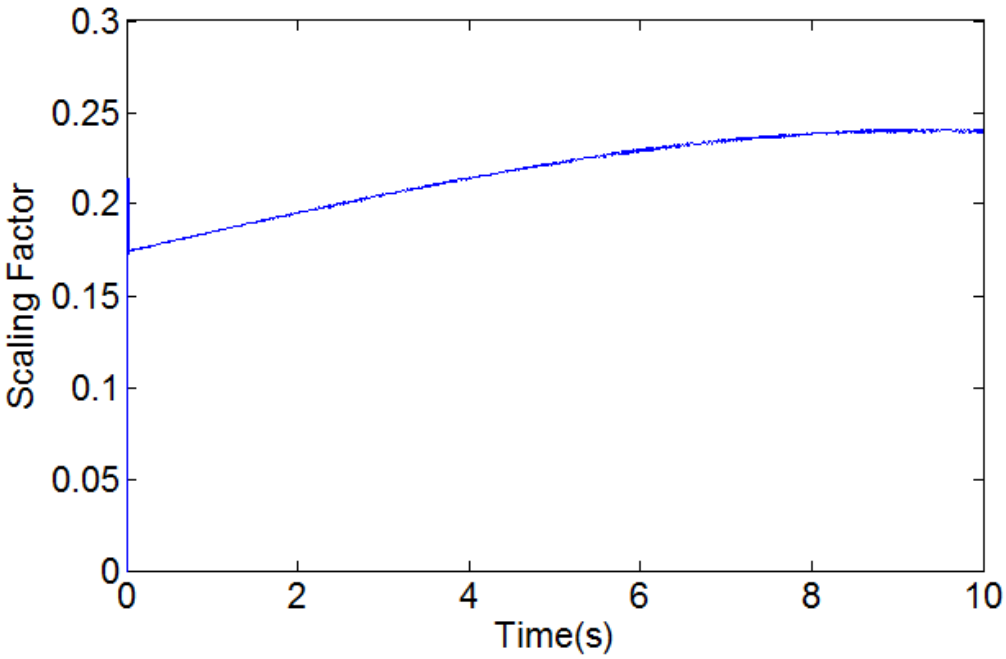

(b)

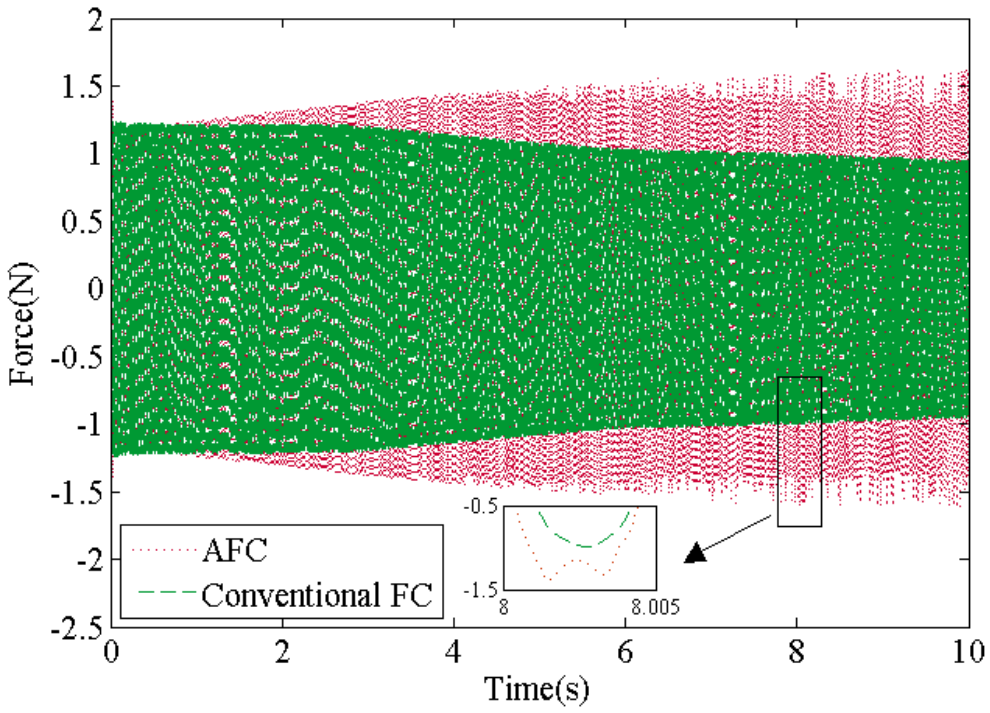

(c)

Fig. 13. Regulation processes of the AFC's factors under frequency-varying excitation: (a) quantification factor I, (b) scaling factor, and (c) output force of controlle

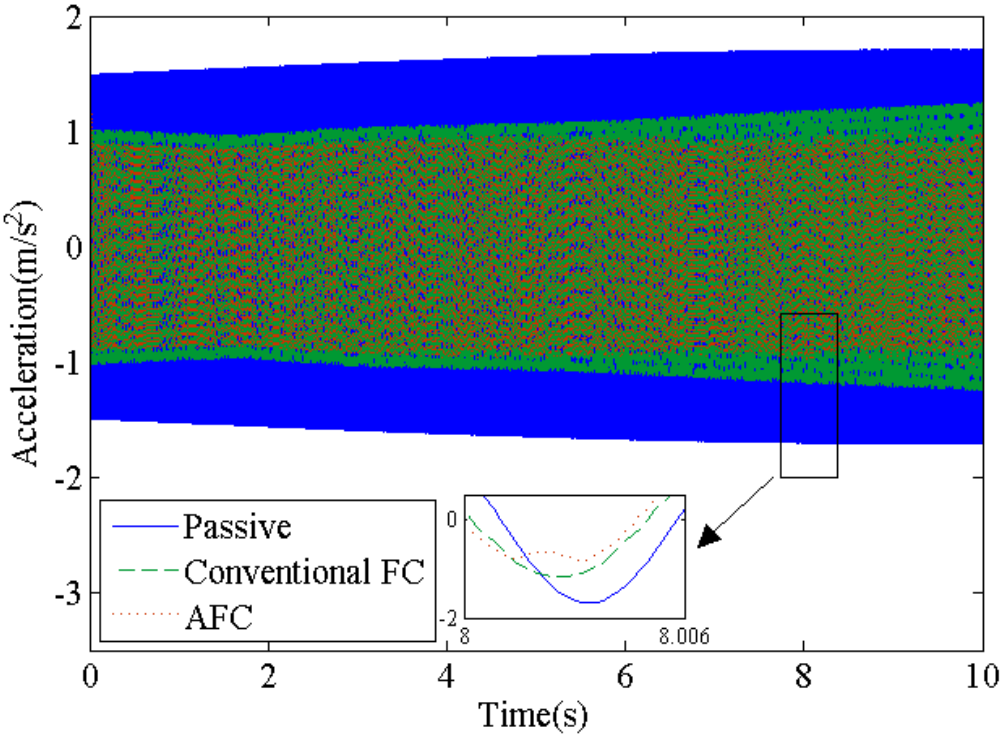

(a)

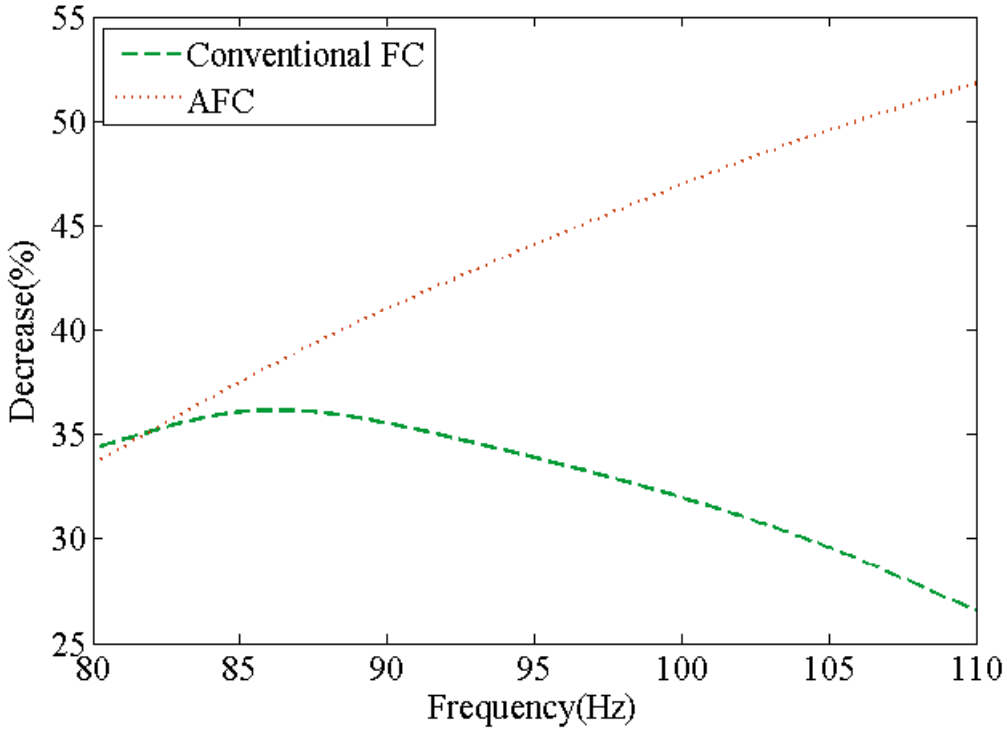

(b)

Fig. 14. The isolation structure's acceleration under different controllers and frequency-varying excitation: (a) responses in time domain, and (b) percentage decreases

4.3 Sinusoidal excitation varying in both amplitude and frequency

The amplitude of the sinusoidal excitation increases from 1.0 to 4.0 m/s^2 in 10

seconds linearly while the frequency increases from 80 to 110 Hz. The regulation processes of the AFC's quantification factor I and scaling factor are shown in Fig. 15. And Fig. 16 compares the responses and percentage decreases of the isolation structure's acceleration under different controllers. The RMS values and percentage decreases of accelerations with respect to the passive isolator in each case are summarized in Table 4. It can be seen from Fig. 16 and Table 4 that the more difference in increasing magnitude from the initial excitation (1m/s&80Hz) is, the lower percentage decrease the conventional FC can achieve, but the greater percentage the AFC can accomplish, the percentage's difference is even as high as 44.66 % at most.

Table 4 Simulation results comparison of the isolation structure accelerations with excitation varying in both amplitude and frequency under different controllers

Excitation Frequency (Hz)	Excitation Amplitude (m/s^2)	FC Decrease (%)	AFC Decrease (%)
80	1	34.32	33.65
85	1.5	35.01	37.88
90	2	25.78	41.05
95	2.5	10.22	43.07
100	3	2.816	44.11
105	3.5	0.3163	44.59
110	4	0.3393	44.66

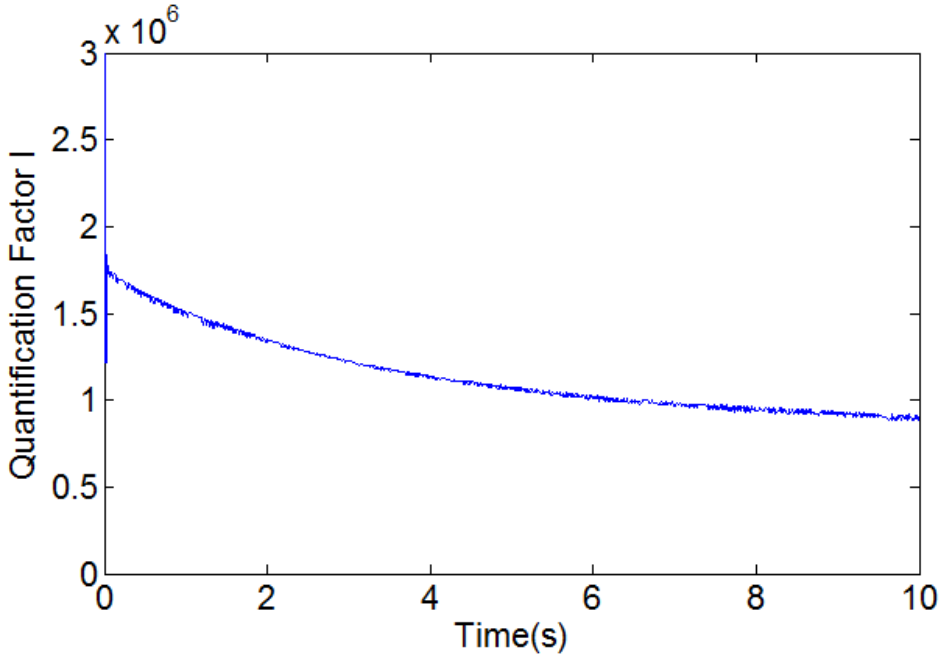

(a)

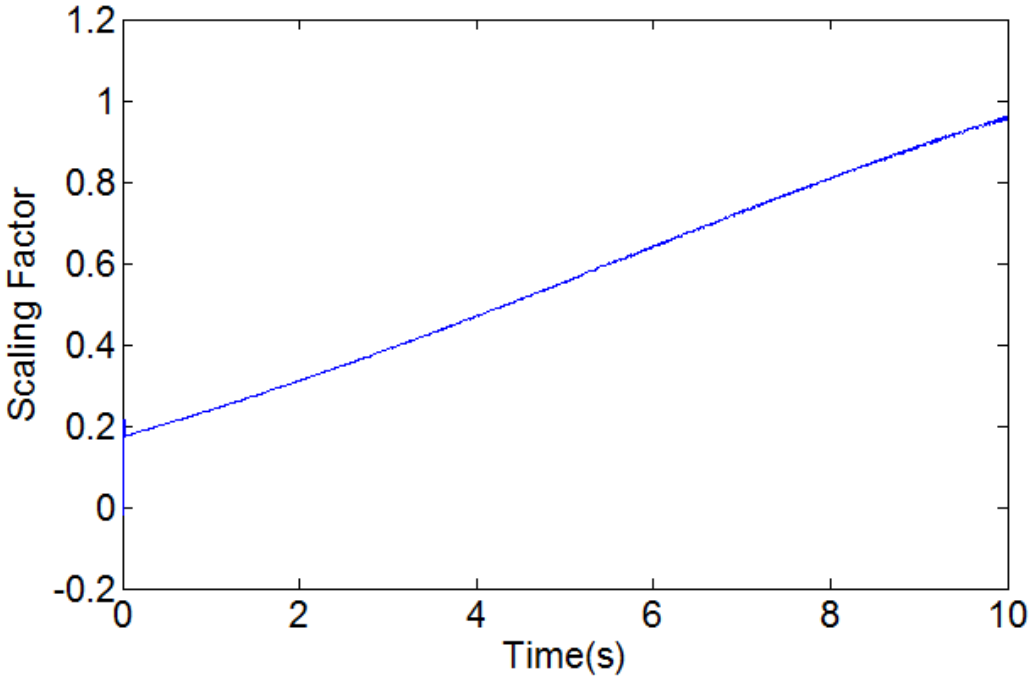

(b)

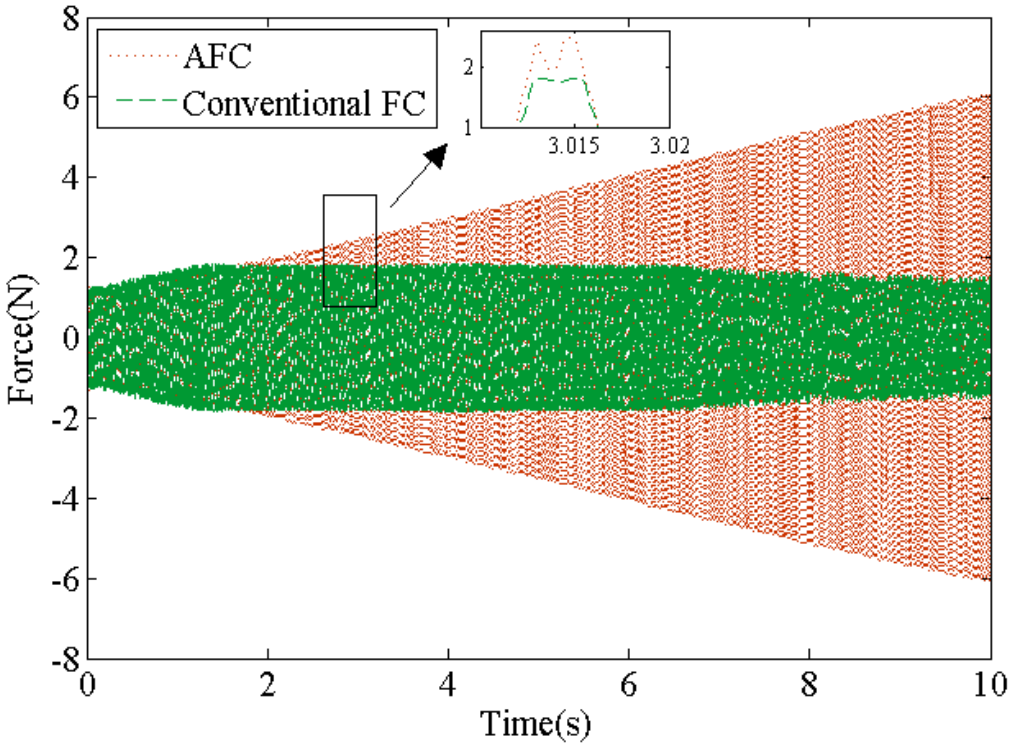

(c)

Fig. 15. Regulation processes of the AFC's factors under sinusoidal excitation varying in both amplitude and frequency: (a) quantification factor I, (b) scaling factor, and (c) output force of controller

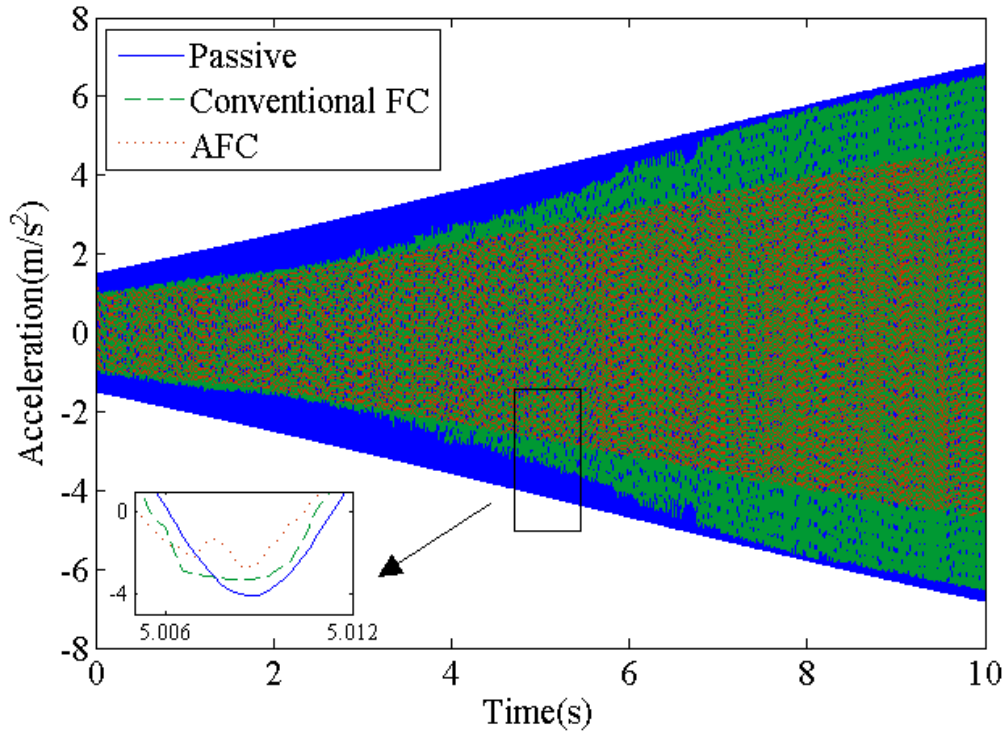

(a)

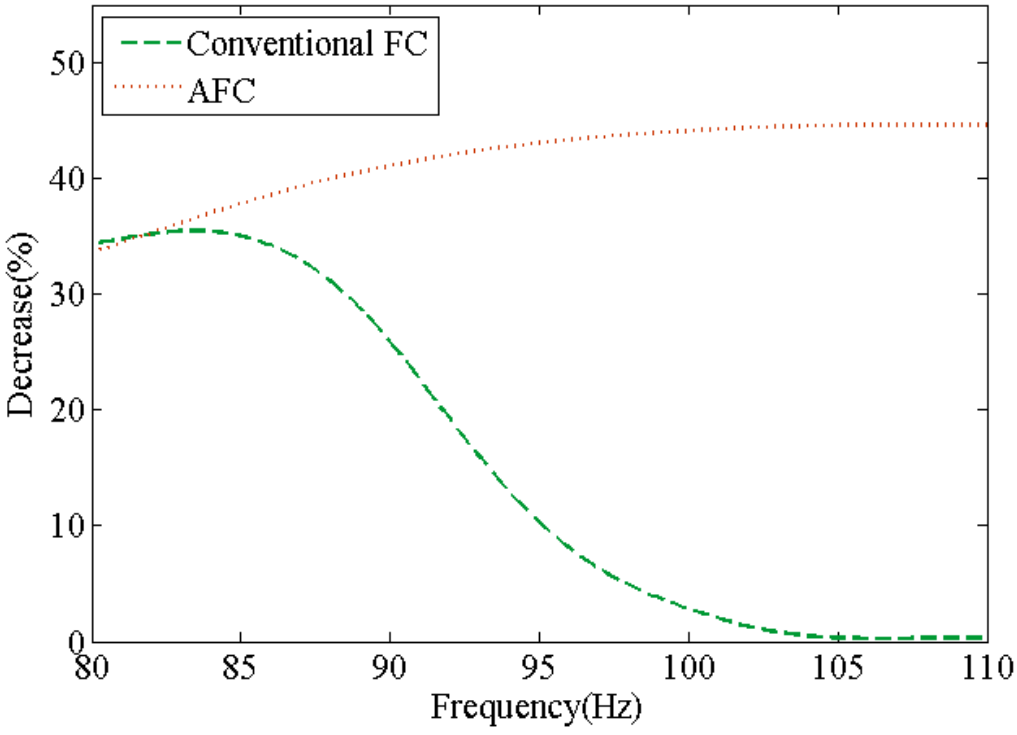

(b)

Fig. 16. The isolation structure's acceleration under different controllers and sinusoidal excitation varying in both amplitude and frequency:

(a) responses in time domain, and (b) percentage decreases

5. Experimental verification

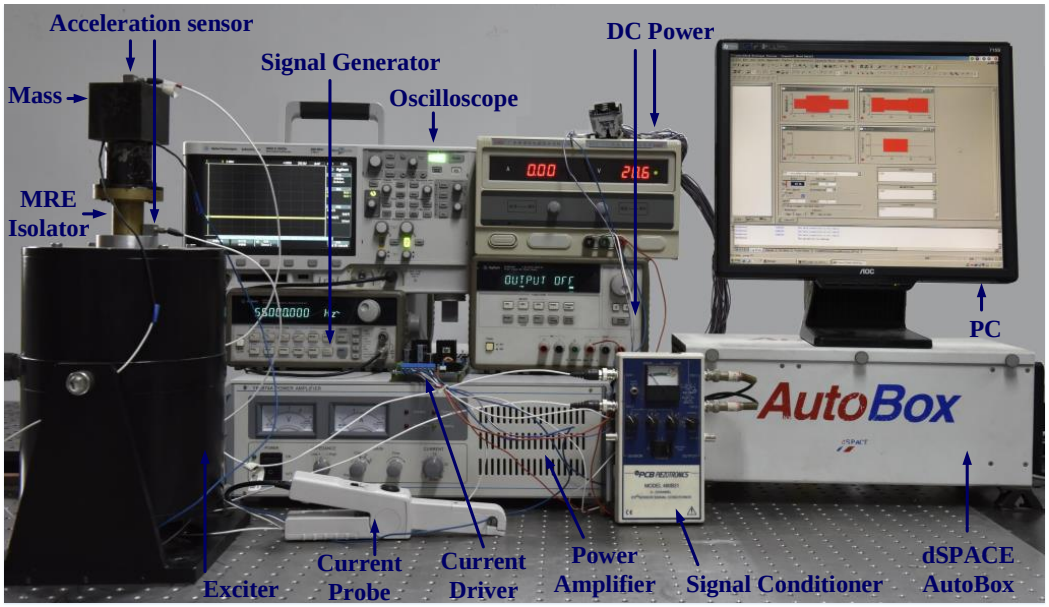

(a)

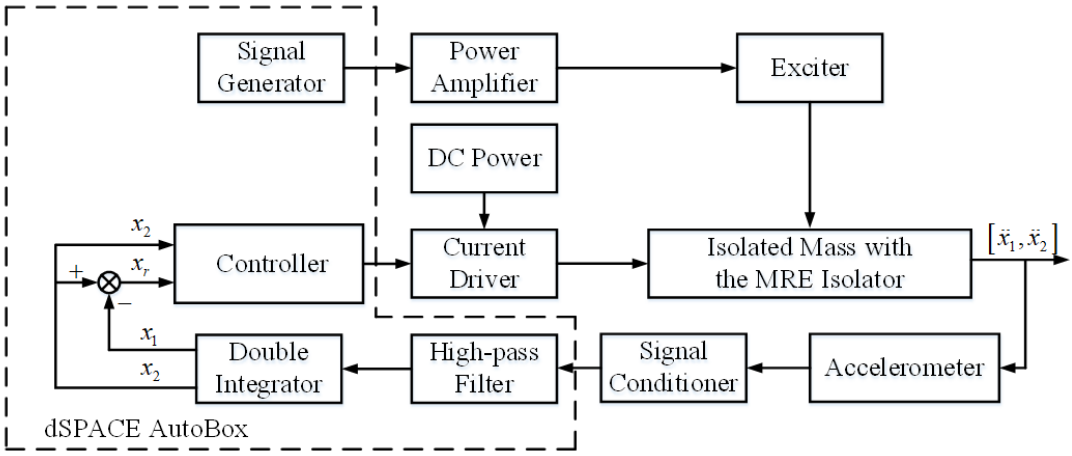

(b)

Fig. 17. Experimental setup for MRE vibration isolation control system with AFC: (a) photograph, and (b) schematic configuration

The AFC method developed for the MRE isolation system in this paper is evaluated experimentally, and the experimental setup is shown in Fig. 17.

The MRE isolator is mounted on the top of exciter (Model JZK-50, Sinocera Piezotronics, China). The desired signal waveform applied to the isolation system is generated by the Simulink model and output by the dSPACE AutoBox (Model ds1005, dSPACE, Germany) via power amplifier (Model YE5874, Sinocera Piezotronics, China) to drive the exciter. A load which represents the precision vibration isolation system is fixed on the mounting plate of the isolator. Two same accelerometers (Model 333B52, Piezotronics, USA) are mounted on the excitation plate and the load to measure the accelerations of the excitation and the isolation

structure, respectively. After being conditioned and filtered, the absolute displacement and relative displacement of the isolation structure can be obtained through the double integrator and then sent to the designed AFC. The current driver converts the control voltage output by the controller to the control current to drive the magnet-exciting coil in MRE isolator. Two DC power supplies (Model E3631A, Agilent, USA) are used to power the current driver.

5.1 Amplitude-varying excitation for a fixed frequency

In each experiment, the basic excitation acceleration signal is increased from 1.0 m/s^2 to 4.0m/s^2 with the step of 0.5m/s^2 under excitation frequency 80Hz. The acceleration responses, control voltage and decrement percentage for amplitude-varying excitation and frequency 80Hz under different controllers are shown in Figs. 18 and 19, respectively. It can be obtained from figures that the performance of AFC has advantage over the conventional FC and passive controller. Especially when the amplitude of acceleration is greater than 1.5m/s^2, the acceleration responses with conventional FC are obviously deteriorated, and even enlarge the acceleration response of isolate structure in comparison with passive control.

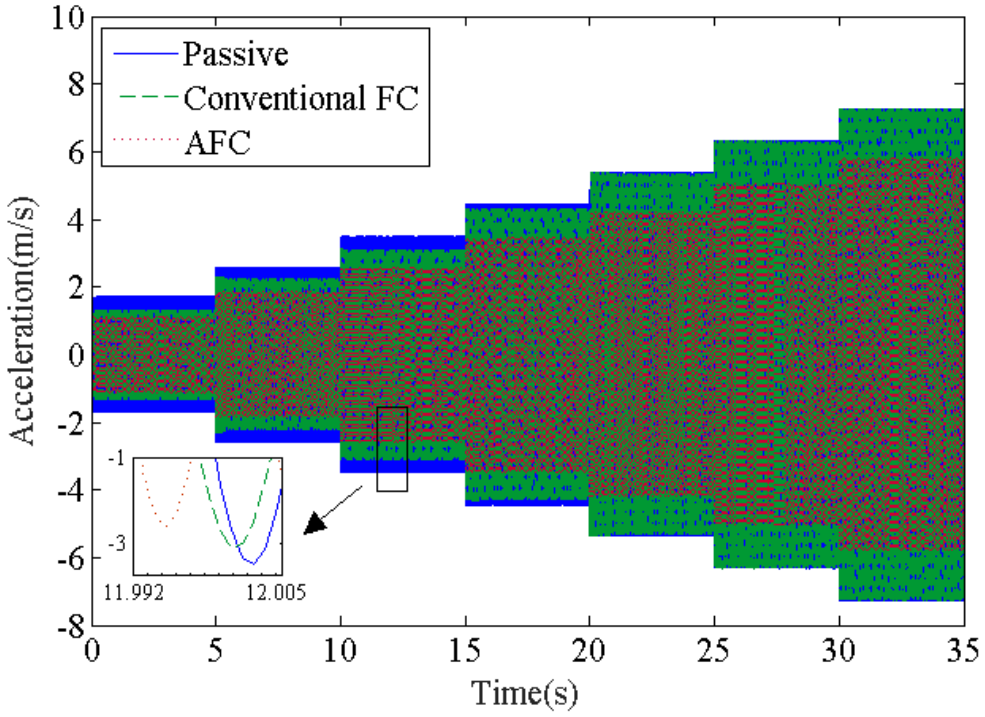

(a)

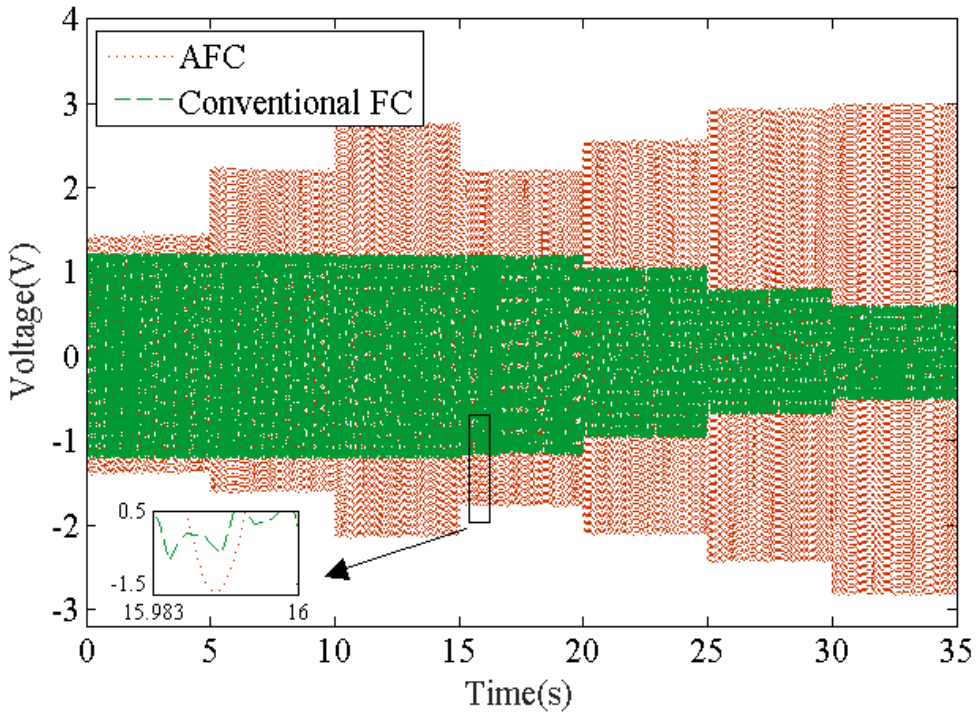

(b)

Fig. 18. Experimental results with amplitude-vary excitation and 80Hz: (a) acceleration response, and (b) control voltage

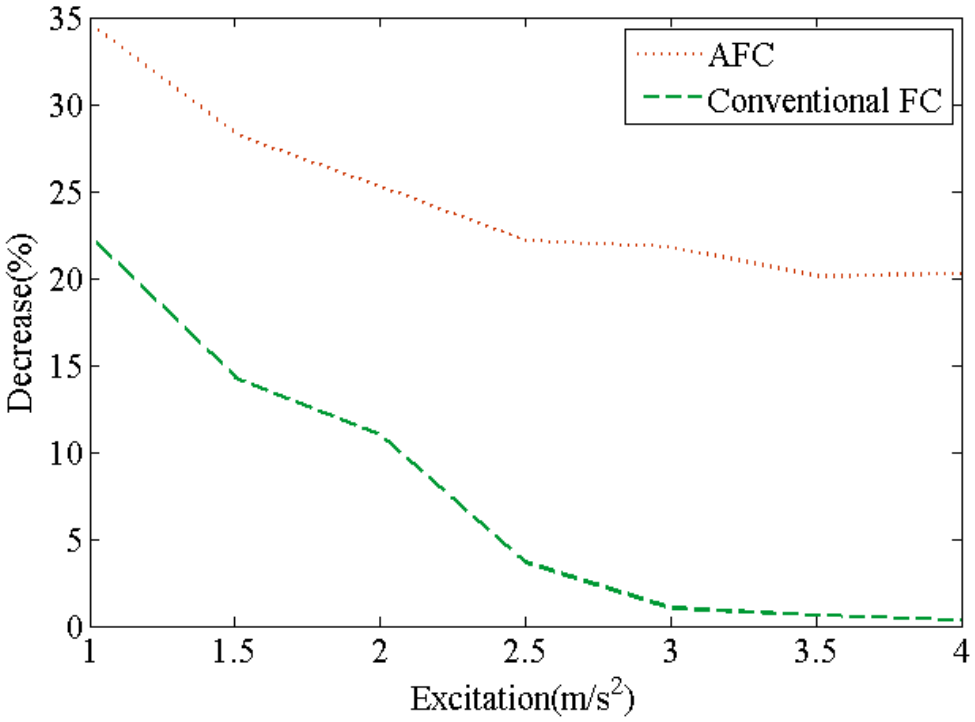

Fig.19. Decrement percentage with amplitude-varying excitation at frequency 80Hz under different controllers

5.2 Frequency-varying excitation for the constant excitation amplitude

In this section the excitation's amplitude is fixed at 1m/s^2 and frequency changes from 80Hz to 110Hz with the step of 5Hz. The experimental results under different controllers are shown in Figs. 20 and 21. It can be seen that the decrement of acceleration RMS with AFC can always more than that with conventional FC. Therefore, the AFC outperforms the conventional FC for fixed amplitude (1m/s^2) and variable frequency (80-100Hz) excitation.

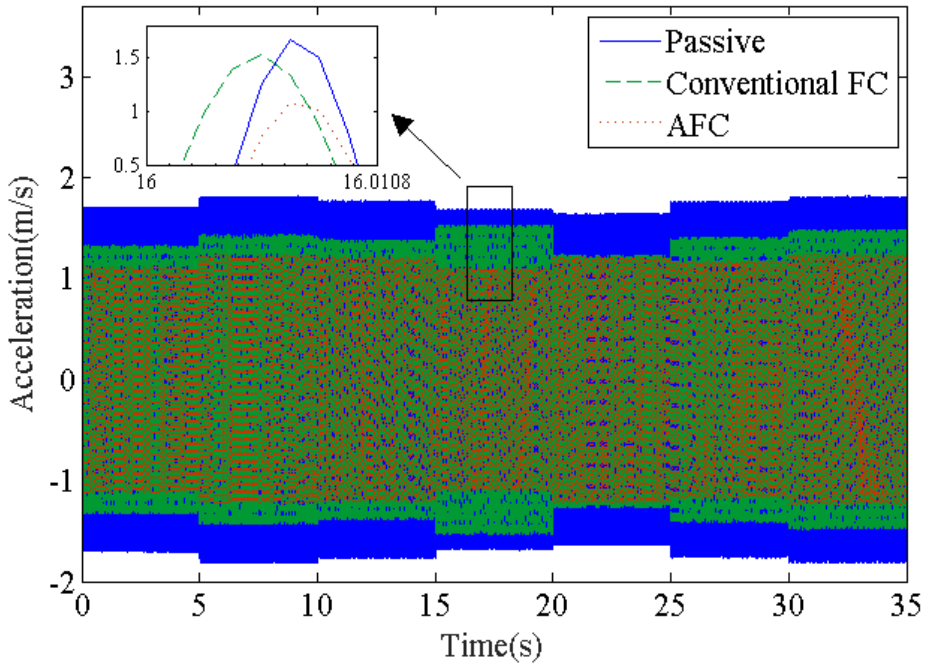

(a)

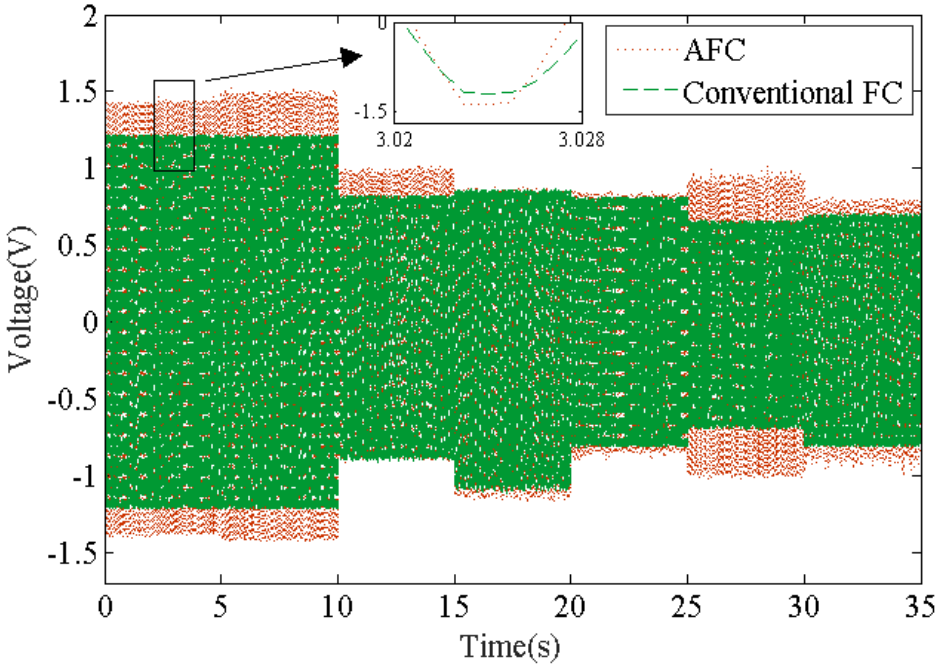

(b)

Fig. 20. Experimental results under frequency-varying excitation and amplitude of 1m/s^2: (a) acceleration response, and (b) control voltage

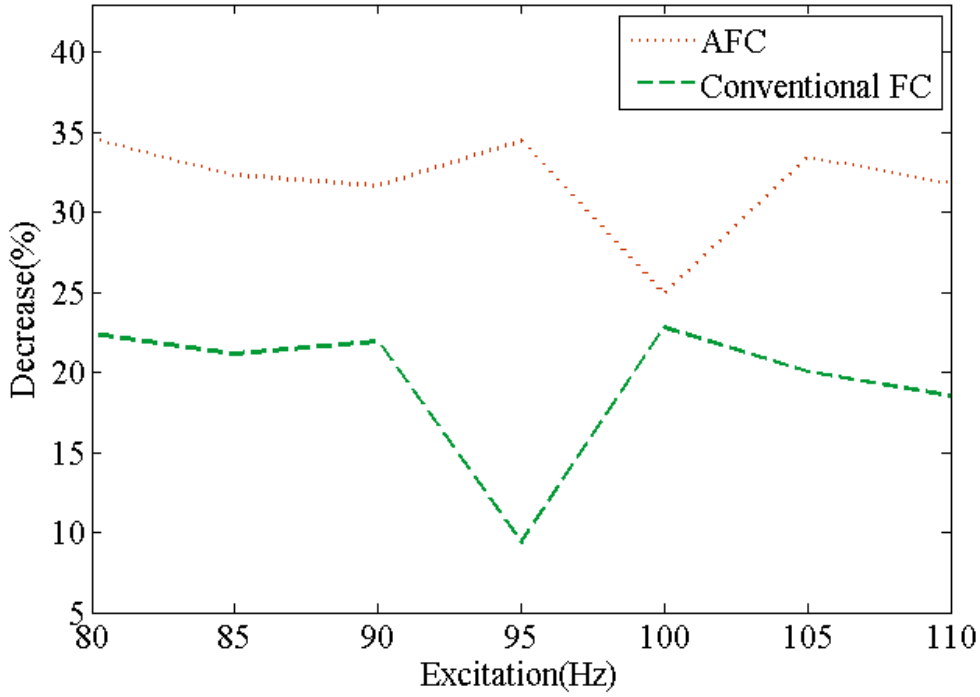

Fig. 21. Percentage decrease with frequency-varying excitation at excitation amplitude at1m/s^2 under different controllers

5.3 Sinusoidal excitation varying in both amplitude and frequency

The experimental results under excitation with variable amplitude (1m/s^2-4 m/s^2) and frequency (80 Hz-110Hz) and different controllers are shown in Figs. 22 and 23. The RMS values and percentage decreases of accelerations with respect to the passive isolator in each case are summarized in Table 5. The results show that the acceleration RMS with AFC decreases at least 13.58%, and always more than the value with FC. In addition, the value with FC decreases sharply with the increasing excitation amplitude, and is only 1.18% at 4m/ s^2. Therefore, it can draw the conclusion that AFC has a strong ability to suppress vibration for a complex time-varying excitation, and the effectiveness and superiority of the designed AFC are validated experimentally.

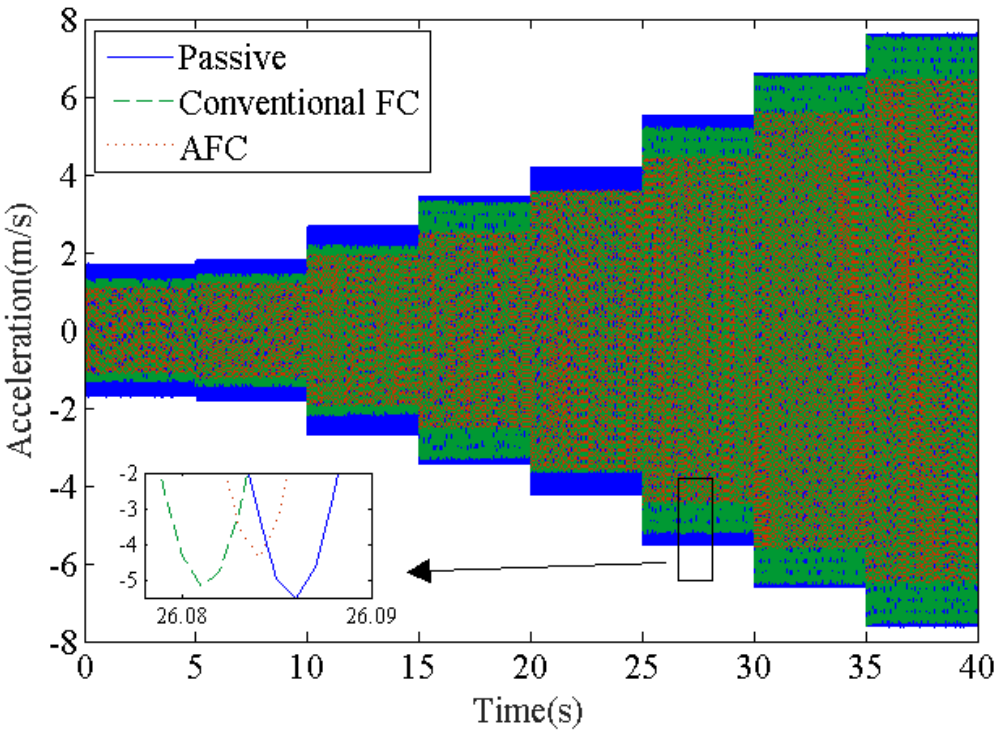

(a)

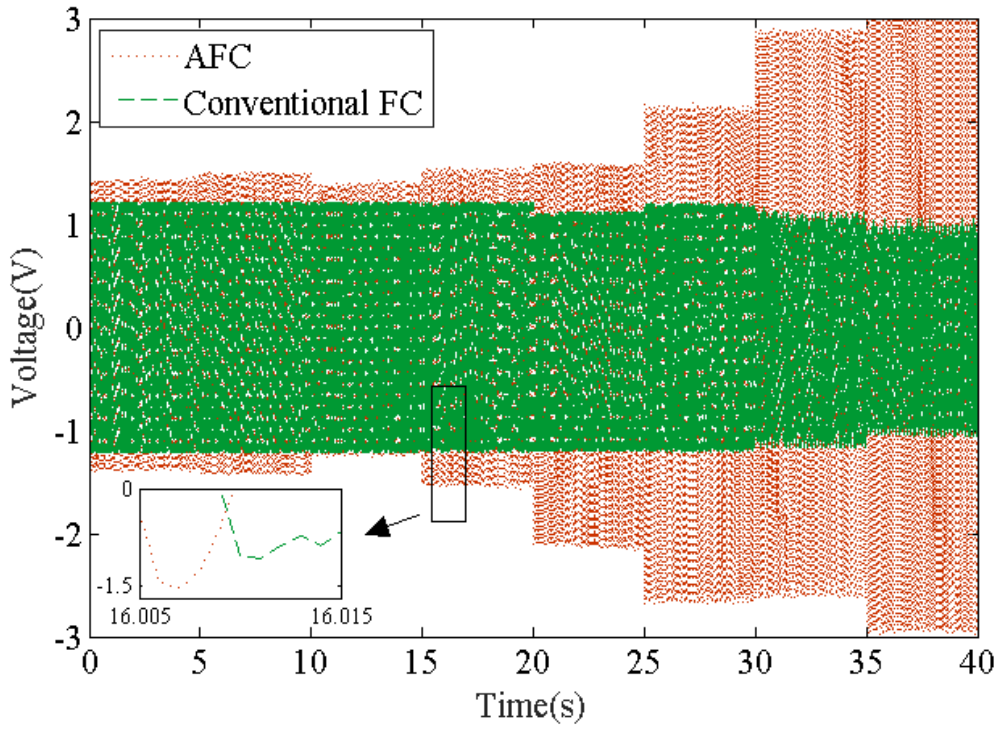

(b)

Fig. 22. Experimental results with excitation varying in both amplitude and frequency under different controllers: (a) acceleration response, and (b) control voltage

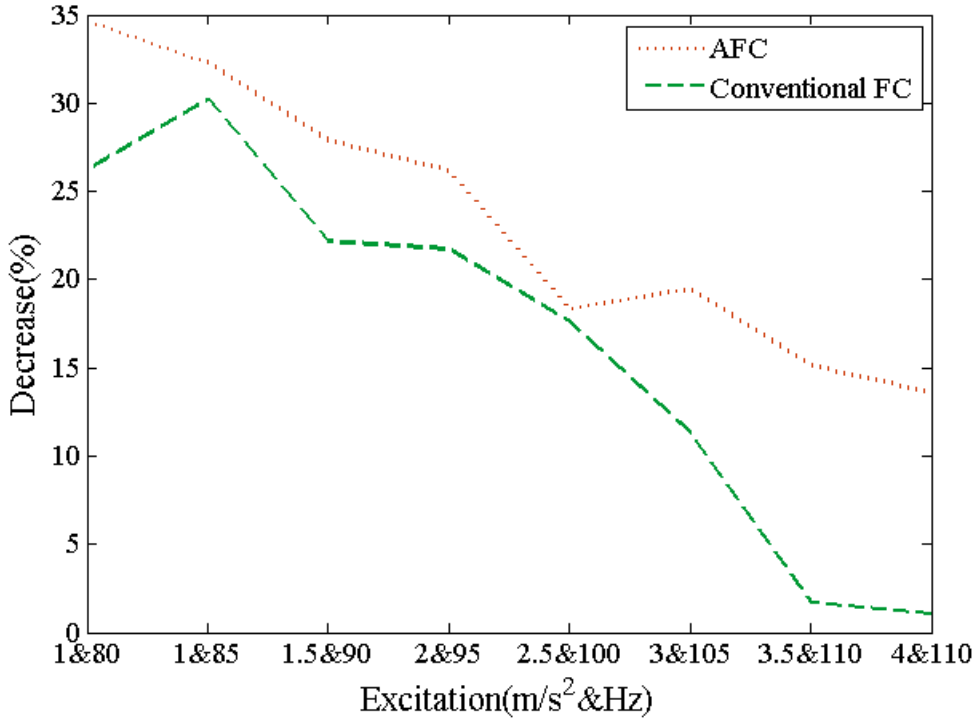

Fig. 23. Percentage decrease with excitation varying in both amplitude and frequency under different controllers

Table 5 Experimental results comparison of the isolation structure accelerations with excitation varying in both amplitude and frequency under different controllers

Excitation Frequency (Hz)	Excitation Amplitude (m/s^2)	Passive	FC		AFC	
		RMS (m/s^2)	RMS (m/s^2)	Decrease (%)	RMS (m/s^2)	Decrease (%)
80	1	1.22	0.90	26.24	0.80	34.65
85	1	1.28	1.01	21.15	0.87	32.31
90	1.5	1.89	1.53	19.16	1.37	27.88
95	2	2.43	2.32	4.29	1.79	26.16
100	2.5	3.01	2.58	14.16	2.46	18.34
105	3	3.91	3.68	5.92	3.15	19.46
110	3.5	4.68	4.60	1.70	3.97	15.13
110	4	5.39	5.23	1.18	4.66	13.58

6. Conclusions

This paper studies the AFC design of an MRE vibration isolation system with time-varying sinusoidal excitations. The MRE isolation system's passive model is obtained

from acceleration sweep experiment. An AFC is devised based on the working principle of the MRE isolator and fuzzy theory, the adaptive mechanism (factor adjustment) of which is constructed on passive system model and peak observer, which is implication of excitation frequency. Experimental results show that the decrease of the isolation structure acceleration under the AFC is 34.65% higher at most than the one of given by the conventional FC. And the AFC could maintain consistent performance in the presence of time-varying excitation parameters (amplitude from 1.0 m/s^2 to 4.0 m/s^2, and frequency from 80Hz to 110Hz) while the conventional FC with constant factors only achieves satisfying control effect around the initial design condition. The results presented in this work are quite self-explanatory justifying that the proposed AFC can be also used to vibration control of various smart structures subject to time-varying excitations in which both amplitudes and frequencies are changing during control action.

Acknowledgements

This research was supported by the National Natural Science Foundation of China (grant no. 51875056, 51775064), Joint Fund of Equipment Pre-research of Education Ministry (grant no. 6141A02022108). The authors are grateful for the helpful comments from the reviewers and editor to improve the paper.

References

[1] H. Yoshioka, Y. Takahashi, K. Katayama, et al. An active microvibration isolation system for hi-tech manufacturing facilities. *Journal of Vibration and Acoustics-Transactions of the ASME*, 123 (2001) 269-275.

[2] Y. L. Xu, Z F. Yu, S. Zhan. Experimental study of a hybrid platform for high-tech equipment protection against earthquake and microvibration. *Earthquake Engineering & Structural Dynamics*, 37 (2007) 747-767.

[3] D. D. Jang, H J. Jung, Y H. Shin, et al. Feasibility study on a hybrid mount system with air springs and piezo-stack actuators for microvibration control. *Journal of Intelligent Material Systems and Structures*, 23 (2012) 515-526.

[4] S. H. Kim, S B. Choi, S R. Hong, et al. Vibration control of a flexible structure using a hybrid mount. *International Journal of Mechanical Sciences*, 46 (2004) 142-157.

[5] J. D. Carlson, M R. Jolly. MR fluid, foam and elastomer devices. *Mechatronics*, 10 (2000) 555-569.

[6] C. Lin, X. L. Gong, W. Q. Jiang, et al. Investigation on magnetorheological elastomers based on natural rubber. *Journal of Materials Science*, 42 (2007) 5483-5489.

[7] M. Yu, M. Zhu, J. Fu, et al. A dimorphic magnetorheological elastomer incorporated with Fe nano-flakes modified carbonyl iron particles: preparation and characterization. *Smart Materials and Structures*, 24 (2015) 115021.

[8] M. Yu, S. Qi, J. Fu, et al. A high-damping magnetorheological elastomer with bi-directional magnetic-control modulus for potential application in seismology. *Applied Physics Letters,* 107 (2015) 035005.

[9] H. Du, W. Li, N. Zhang. Semi-active variable stiffness vibration control of vehicle seat suspension using an MR elastomer isolator. *Smart Materials and Structures*, 20 (2001) 105003.

[10] U C. Jeong, J H. Yoon, I H. Yang, et al. Magnetorheological elastomer with stiffness-variable characteristics based on induced current applied to different mount of vehicles. *Smart Materials and Structures*, 22 (2013) 115007.

[11] W. H. Li, X. Z. Zhang, H. P. Du. Development and simulation evaluation of a magnetorheological elastomer isolator for seat vibration control. *Journal of Intelligent Material Systems and Structures*, 23 (2015) 1041-1048.

[12] S. S. Sun, J. Yang, H. X. Deng, et al. Horizontal vibration reduction of a seat suspension using negative changing stiffness magnetorheological elastomer isolators. *International Journal of Vehicle Design*, 68 (2015) 104-118.

[13] J. Fu, M. Yu, X. M. Dong, et al. Magnetorheological elastomer and its application on impact buffer. *Journal of Physics Conference series.* 412 (2013) 012032.

[14] J. Fu, Y. Wang, P D. Li, et al. Research on hybrid isolation system for micro-nano-fabrication platform. *Advances in Mechanical Engineering*, (2014) 24247.

[15] V. P. Mikhailov, A. M. Bazinenkov. A vibration-control platform on the basis of magnetorheological elastomers. *Instruments and Experimental Techniques*, 59 (2016) 131-135.

[16] J. Fu, P. D. Li, Y. Wang, et al. Model-free fuzzy control of magnetorheological elastomer vibration isolation system: analysis and experimental evaluation. *Smart Materials and Structures*, 25 (2016) 035030.

[17] Z.D. Xu, S. Suo, Y. Lu. Vibration control of platform structures with magnetorheological elastomer isolators based on an improved SAVS law, *Smart Materials and Structures,* 25 (2016) 065002.

[18] H. J. Jung, S. H. Eem, D. D. Jang, et al. Seismic performance analysis of a smart base-

isolation system considering dynamics of MR elastomers. *Journal of Intelligent Material Systems and Structures*, 22 (2011) 1439-1450.

[19] M. Behrooz, X. Wang, Gordaninejad F. Modeling of a new semi-active/passive magnetorheological elastomer isolator. *Smart Materials and Structures*, 23 (2014) 045013.

[20] M. Behrooz, X. Wang, F. Gordaninejad. Performance of a new magnetorheological elastomer isolation system. *Smart Materials and Structures*, 23 (2014) 045014.

[21] J. Yang, S. S. Sun, H P Du, et al. A novel magnetorheological elastomer isolator with negative changing stiffness for vibration reduction. *Smart Materials and Structures*, 23 (2014) 105023.

[22] J. Yang, S.S. Sun, T F. Tian, et al. Development of a novel multi-layer MRE isolator for suppression of building vibrations under seismic events. *Mechanical Systems and Signal Processing*, (2016) 70-71:811-820.

[23] X.Y. Gu, Y. Yu, J. C. Li, et al. Semi-active control of magnetorheological elastomer base isolation system utilising learning-based inverse model. *Journal of Sound and Vibration*, 406 (2017) 346-362.

[24] Y.Q. Ni, Z.G. Ying, Z.H. Chen. Micro-vibration suppression of equipment supported on a floor incorporating magneto-rheological elastomer core. *Journal of Sound and Vibration*, 330(2011) 4369-4383.

[25] B. Nayak, S.K. Dwivedy, K.S.R.K. Murthy. Dynamic analysis of magnetorheological elastomer-based sandwich beam with conductive skins under various boundary conditions. *Journal of Sound and Vibration*, 330 (2011) 1837-1859.

[26] B. X. Ju, M. Yu, J. Fu, et al. A novel porous magnetorheological elastomer: preparation and evaluation. *Smart Materials and Structures*, 21 (2012) 290-298.

[27] S. Opie, W. Yim. Design and control of a real-time variable modulus vibration isolator. *Journal of Intelligent Material Systems and Structures*, 22 (2011) 113-125.

[28] G. J. Liao, X. L. Gong, S. H. Xuan, et al. Development of a real-time tunable stiffness and damping vibration isolator based on magnetorheological elastomer. *Journal of Intelligent Material Systems and Structures*, 23 (2012) 25-33.

[29] T. H. Lee, H. K. Lam, F. H. F. Leung, et al. A practical fuzzy logic controller for the path tracking of wheeled mobile robots. *IEEE Control Systems Magazine,* 23 (2003) 574-579.

[30] M. Yu, S. B. Choi, X. M. Dong, et al. Fuzzy neural network control for vehicle stability utilizing magnetorheological suspension system. *Journal of Intelligent Material Systems and Structures*, 20 (2009) 457-466.

[31] S. D. Nguyen, Q. H. Nguyen, S. B. Choi. A hybrid clustering based fuzzy structure for

vibration control-Part 2: An application to semi-active vehicle seat-suspension system. *Mechanical Systems and Signal Processing*, 56 (2015) 288-301.

[32] N. D. Zorić, A. M. Simonović, Z. S. Mitrović, et al. Free vibration control of smart composite beams using particle swarm optimized self-tuning fuzzy logic controller. *Journal of Sound and Vibration*, 333 (2014) 5244-5268.

[33] R. K. Mudi, N. R. Pal. A self-tuning fuzzy PI controller. *Fuzzy Sets and Systems*, 115 (2000) 327-338.

[34] J. H. Park, G. T. Park, S. H. Kim, et al. Direct adaptive self-structuring fuzzy controller for nonaffine nonlinear system. *Fuzzy Sets and Systems*, 153 (2005) 429-445.

[35] P. M. Mary, N. S. Marimuthu. Design of self-tuning fuzzy logic controller for the control of an unknown industrial process. *IET Control Theory and Applications*, 3 (2009) 428-436.

[36] J. Fu, G. Y. Liao, P. D. Li, et al. NARX neural network modeling and robustness analysis of magnetorheological elastomer isolator. *Smart Materials and Structures*, 25 (2016) 125019.

[37] C. Y. Yang, J. Fu, X. Zheng, et al. A new magnetorheological elastomer isolator in shear-compression mixed mode. *Journal of Intelligent Material Systems and Structures*, 26 (2015) 1290-1300.